

Molten Globule-like Conformation of Barstar: A Study by Fluorescence Dynamics

R. Swaminathan,[†] N. Periasamy,^{*†} Jayant B. Udgaonkar,[‡] and G. Krishnamoorthy^{*†}

Chemical Physics Group, Tata Institute of Fundamental Research, Homi Bhabha Road, Bombay 400 005, India, and National Centre for Biological Sciences, T.I.F.R. Centre, Indian Institute of Science Campus, P.O. Box 1234, Bangalore 560 012, India

Received: March 18, 1994; In Final Form: June 3, 1994[⊙]

Time-resolved fluorescence intensity and anisotropy decay measurements have been carried out on barstar, the inhibitor protein of the bacterial ribonuclease, barnase. The intrinsic fluorescence of the three tryptophans in this protein have been used to characterize the molten globule-like conformation at pH 3 (A form) and the native conformation at pH 7 (N state). The fluorescence intensity decay could be fitted to a sum of two exponentials with lifetimes of 4.1 and 1.5 ns at pH 7 (N state) and three exponentials with lifetimes of 4.9, 1.5, and 0.2 ns at pH 3 (A form). The emergence of the 0.2-ns component was pH dependent with a pK of ~ 4.5 . Fluorescence quenching by iodide has shown that the tryptophan (Trp) residues are solvent inaccessible at pH 7 and partially exposed at pH 3 (A form). Quenching by acrylamide has suggested that the 1.5-ns decay component arises from one of the three Trp residues and the 4.1-ns component arises from the remaining two Trp residues. Of the latter, one is buried and the other is highly accessible to acrylamide. Decay of fluorescence anisotropy has shown that the Trp residues are rigidly held and do not have any segmental mobility at pH 7. The A form is characterized by a high level of aggregation and a high degree of internal motion. The aggregated A form could be relevant in the folding pathway of barstar when the possibility of interaction of molten globular form with chaperone proteins is recognized. Comparison of the dynamic behavior of the Cys \rightarrow Ala mutant with that of the wild type has shown the proximity of SH group(s) to Trp residues.

Introduction

The protein-folding problem, namely, the mechanism by which a linear polypeptide chain is transformed into a well-defined, complex, three-dimensional structure, has attracted wide attention in recent years.^{1–3} Most of the studies have been focused on establishing the structural characteristics of the intermediates involved in the folding pathway.^{4–6} In this respect, the partly folded conformational state of the protein, commonly termed as the molten globule, has received widespread interest (see ref 7 for a recent review).

The molten globule state, which is stabilized at the extremes of pH and ionic strength,^{8,9} is characterized by a compact and well-defined secondary structure and the presence of very little tertiary structure.^{7,10,11} Although there has been little evidence to establish the presence of the molten globule state as a kinetic intermediate in the folding pathway, investigations on its structure have been pursued with the aim of obtaining some vital clues about protein structure during the early stages of folding.^{4,10} The molten globule state of proteins such as α -lactalbumin, apomyoglobin, and cytochrome *c* have been very well characterized (ref 7 and the references cited therein). All of them seem to have certain common features, which is why the molten globule is now regarded as a universal intermediate in the folding pathway.⁷

Our studies have concentrated on the bacterial ribonuclease inhibitor protein barstar. Barstar is an 89 amino acid residue protein of molecular weight 10 100 produced naturally by *Bacillus amyloliquefaciens*.¹² Equilibrium unfolding studies of barstar¹³ have shown the existence of two conformations, one of which closely resembles the molten globule. This form is stabilized at low (<4) pH values. Barstar has three tryptophans. Their intrinsic fluorescence can be used in gaining insight into structural and dynamic aspects of the protein.¹⁴ We report here the time-resolved intrinsic fluorescence studies on the native, denatured, and putative molten globule states of barstar. Fluorescence

lifetimes, which are obtained from the time-resolved fluorescence decays, provide useful information regarding the interaction of the fluorophore with the surrounding environment. The tryptophan (Trp) residue in proteins has a fluorescence lifetime in the range 0.1–10 ns.¹⁵ Events that occur in this time scale include motion of the whole protein and segmental motion around the Trp residue. These events which can be monitored from the time-resolved anisotropy decay studies could be correlated with structural and dynamic aspects of the protein. Our studies have shown that the low pH form of barstar is characterized by a high level of internal mobility and a high degree of aggregation.

Experimental Section

Barstar was obtained by expression of plasmid pMT316 (a generous gift of Dr. R. W. Hartley), having the barstar structural gene under control of the *tac* promoter, in the transformed *Escherichia coli* strain MM294. The expressed protein was subsequently purified.¹³ All the chemicals used in the experiments were of Analar grade. Guanidine hydrochloride (GdnHCl) was obtained from Sigma (Molecular Biology Reagent grade). Stock solutions of urea were made fresh on the day of use.

Time-Resolved Fluorescence and Anisotropy Decay Measurements. Time-resolved fluorescence decay of barstar was observed by employing a CW mode-locked frequency-doubled Nd-YAG laser-driven dye (Rhodamine 6G) laser operating at a repetition rate of 800 kHz with pulse width of the order of 4–10 ps and tunability in the region of 570–640 nm (see ref 16 for a detailed description). Fluorescence decay curves were obtained by using a time-correlated single-photon-counting setup¹⁶ coupled to a microchannel plate photomultiplier (Model 2809U; Hamamatsu Corp.). The instrument response function (IRF) was obtained at 295 nm using a dilute colloidal suspension of dried nondairy coffee whitener. The half-width of the IRF was ~ 100 ps.¹⁷ The protein was excited at 295 nm using the second harmonic output of the dye laser from an angle-tuned KDP crystal, and the fluorescence emission was collected through a 320-nm cut-off filter followed by a monochromator. The cut-off filter was used to prevent scattering of the excitation beam from the protein

* Authors for correspondence.

[†] Tata Institute of Fundamental Research.

[‡] National Centre for Biological Sciences.

[⊙] Abstract published in *Advance ACS Abstracts*, August 15, 1994.

samples. The peak counts obtained in control experiments were comparable to the background level. In fluorescence lifetime measurements, the emission was monitored at the magic angle (54.7°) to eliminate the contribution from the decay of anisotropy. In time-resolved anisotropy measurements, the emission was collected at directions parallel (I_{\parallel}) and perpendicular (I_{\perp}) to the polarization of the excitation beam. The anisotropy was calculated as

$$r(t) = \frac{I_{\parallel} - I_{\perp} G(\lambda)}{I_{\parallel} + 2I_{\perp} G(\lambda)} \quad (1)$$

where $G(\lambda)$ is the geometry factor at the wavelength (λ) of emission. The G factor of the emission collection optics was determined in separate experiments using a standard sample (laser dye BMQ dissolved in ethanol) for which the rotational correlation time was 0.23 ns and fluorescence lifetime was 0.83 ns.

The fluorescence decay curves at the magic angle were analyzed by deconvoluting the observed decay with the IRF to obtain the intensity decay function represented as a sum of three exponentials:

$$I(t) = \sum_i \alpha_i \exp(-t/\tau_i) \quad i = 1-3 \quad (2)$$

where $I(t)$ is the fluorescence intensity at time t and α_i is the amplitude of the i th lifetime τ_i such that $\sum_i \alpha_i = 1$.

Fluorescence lifetime distributions were obtained by employing the maximum entropy method (MEM).^{18,19} MEM for fluorescence decay analysis begins with the assumption that the decay represents a distribution of lifetimes ranging from 10 ps to 10 ns (or any other range of 2 or 3 orders), all having equal probability (amplitude). Each iteration in the analysis attempts to arrive at a distribution by minimizing the χ^2 and maximizing the entropy, S (also called the Shannon–Jaynes entropy), which is defined as follows:

$$S = \sum_i -p_i \log p_i \quad (3)$$

where p_i is the probability (amplitude) for the i th lifetime. For a particular value of χ^2 , there will be many possible distributions of p_i ; MEM gives that distribution for which S is maximum. The method will not give structures in the distribution unless warranted by the data. The analysis is terminated if $\chi^2 < 1.0$ or if subsequent iterations have negligible influence on the values of χ^2 and S and the distribution profile. The distribution was displayed in the log τ scale.

The time-resolved anisotropy decay was analyzed based on the model

$$I_{\parallel}(t) = \frac{1}{3}I(t)[1 + 2r(t)] \quad (4)$$

$$I_{\perp}(t) = \frac{1}{3}I(t)[1 - r(t)] \quad (5)$$

$$r(t) = r_0 \sum_i \beta_i \exp(-t/\tau_{ri}) \quad i = 1 \text{ or } 2 \quad (6)$$

where r_0 is the initial anisotropy, β_i is the amplitude of the i th rotational correlation time τ_{ri} such that $\sum_i \beta_i = 1$. In cases where the decay of $r(t)$ was biexponential, τ_{r1} and τ_{r2} represent the internal rotation of Trp residues and the overall tumbling of the protein, respectively. In this model, each τ_i is associated with both τ_{r1} and τ_{r2} . Nonlinear least-squares analysis (Marquardt method) was performed to extract the amplitude parameters α_i , β_i , lifetimes τ_i , and correlation times τ_{ri} .²⁰ In the case of time-resolved anisotropy decay, I_{\parallel} and I_{\perp} were analyzed globally²¹ by using the measured IRF. Since the goodness of fits were satisfactory with two correlation times (τ_{r1} and τ_{r2}), we have not

increased the number of τ_{ri} components to more than two. Fluorescence decay curves were analyzed globally whenever it was found to be appropriate. In the global analysis, several decay curves were simultaneously analyzed for the same τ_i but varying α_i .²²

All the time-resolved measurements involving a systematic variation of a specific experimental condition (e.g., quencher concentration, pH, etc.) were carried out on the same day.

Since the analysis of time-resolved anisotropy decay involves multiparameter fitting with several unknowns, the values obtained from the analysis were employed to calculate the steady-state anisotropy (r_{ss}).

$$r_{ss} = \frac{r_0 \sum_i \sum_j \alpha_i \beta_j \left(\frac{1}{\tau_i} + \frac{1}{\tau_{rj}} \right)^{-1}}{\sum_i \alpha_i \tau_i} \quad (7)$$

This value was compared with the experimentally measured value of the steady-state anisotropy at the same excitation and emission wavelengths under identical conditions. Only the set of parameters which gave the computed steady-state anisotropy value close to the observed value was accepted.

The average angular range of the hindered rotation of the Trp residues was calculated by the model of isotropic diffusion inside a cone.²³ The semiangle θ of the cone was calculated as

$$\theta = \cos^{-1} \left\{ \left(\frac{1}{2} \right) \left[(1 + 8(r_{\infty}/r_0)^{1/2})^{1/2} - 1 \right] \right\} \quad (8)$$

Decay-associated spectra of the individual lifetime components $F_i(\lambda)$ were computed from the steady-state emission spectra ($F(\lambda)$) and the fluorescence decay parameters α_i and τ_i .²⁴

$$F_i(\lambda) = F(\lambda) \left\{ \frac{\alpha_i(\lambda) \tau_i}{\sum_i \alpha_i(\lambda) \tau_i} \right\} \quad (9)$$

Steady-state fluorescence measurements were carried out by using a spectrofluorophotometer (Model RF540; Shimadzu Scientific Instrument Inc.). The slit width for excitation was 5 nm, while that for emission was 10 nm. For measuring the steady-state anisotropy, the L format method²⁵ was followed.

Unless otherwise mentioned, the experiments were carried out at 23–25 °C. Experiments in the presence of denaturants were carried out at least 2 h after the addition of the denaturant. Other details of the experimental method are given in the figure legends.

Results

Fluorescence Lifetime Measurements. Fluorescence Decay in the Absence of Denaturants. The fluorescence decay of Trp residues in barstar at pH 7 can adequately be described as a sum of two exponentials with fluorescence lifetimes of ~ 4.1 and ~ 1.5 ns. Typical decay profiles are shown in Figure 1. The decay parameters for various experimental conditions are given in Table 1. We notice that at pH 3, one needs three exponentials to obtain a good fit, the additional lifetime being ~ 0.2 ns. Also we observed an increase in the value of the longest lifetime from ~ 4.1 ns at pH 7 to ~ 4.9 ns at pH 3.

Apart from the analysis of fluorescence decays by a sum of discrete exponentials (as shown above), the data were also analyzed for a continuous distribution of lifetimes^{26–29} by the maximum entropy method.^{30,31} It has been generally argued that analysis of fluorescence decays by a distribution of lifetimes is more appropriate than fitting them to a sum of a few exponentials especially in the cases of macromolecules and membrane systems.^{32,33}

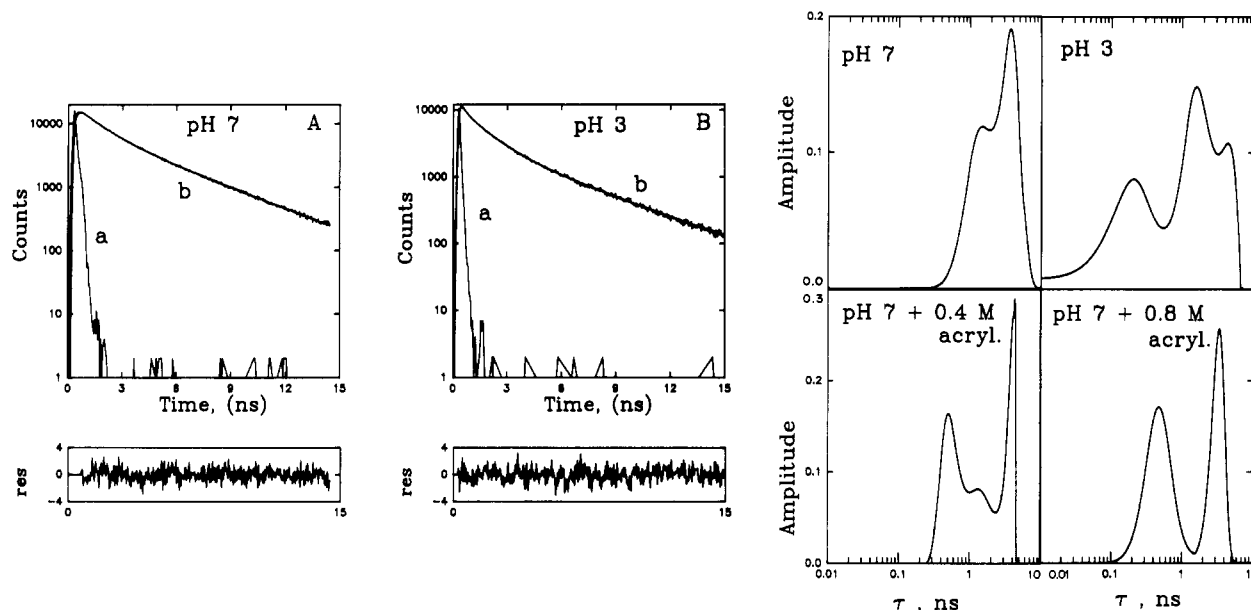


Figure 1. (A and B) Fluorescence intensity decay of barstar at pH 7 (A) and pH 3 (B). The excitation and emission wavelength were 295 and 360 nm, respectively. The concentration of barstar was 30 μ M in 10 mM sodium dihydrogen phosphate, 1 mM EDTA, and 100 μ M dithiothreitol (DTT) for pH 7 and 10 mM glycine, 1 mM EDTA, and 100 μ M DTT for pH 3. The excitation profile (a), emission profile (b), and calculated emission profile (smooth line in b) are shown. The time resolution was 37.8 ps/channel. The deconvoluted lifetimes are 3.94 ns (46%) and 1.32 ns (54%) ($\chi^2_{\text{red}} = 0.91$) at pH 7.0 and 4.83 ns (26%), 1.45 ns (46%), and 0.2 ns (33%) ($\chi^2_{\text{red}} = 1.11$) at pH 3.0. The values given in Table 1 are averages of at least five measurements. The temperature was 25 $^{\circ}$ C. (C) Fluorescence lifetime distributions of barstar analyzed by the maximum entropy method. Profiles corresponding to pH 7.0, 3.0, and 7.0 with either 0.4 M or 0.8 M acrylamide (acryl.) are shown. The χ^2 values in all cases were between 1.0 and 1.1. Other conditions are similar to A and B. Note the emergence of a third (middle) peak at 0.4 M acrylamide.

TABLE 1: Parameters Obtained from the Analysis of Fluorescence Intensity Decays of Barstar and NATA^a

conditions	lifetimes, ns			amplitudes			χ^2_{red}
	τ_1	τ_2	τ_3	α_1	α_2	α_3	
1. barstar at pH 7	4.11	1.46		0.49	0.51		1.28
2. -do- at pH 3	4.88	1.48	0.20	0.21	0.46	0.33	1.15
3. -do- at pH 7 + 6 M GdnHCl	3.57	1.38		0.47	0.53		1.39
4. -do- at pH 3 + 6 M GdnHCl	3.53	1.55	0.24	0.28	0.51	0.21	1.07
5. -do- at pH 7 + 8 M urea	3.92	1.24		0.59	0.41		1.13
6. -do- at pH 3 + 8 M urea	4.03	2.07	0.66	0.24	0.50	0.26	1.14
7. -do- at pH 7 + 5 M GdnSCN	2.85	1.37	0.21	0.33	0.41	0.26	1.18
8. -do- at pH 3 + 5 M GdnSCN	2.53	1.22	0.25	0.30	0.44	0.27	1.15
9. NATA at pH 7	2.79						1.20
10. -do- at pH 3	2.63						1.27
11. -do- at pH 7 + 6 M GdnHCl	2.84						1.03
12. -do- at pH 3 + 6 M GdnHCl	2.80						1.17
13. -do- at pH 7 + 8 M urea	3.91						1.19
14. -do- at pH 3 + 8 M urea	3.24						1.25
15. -do- at pH 7 + 5 M GdnSCN	2.30						1.21
16. -do- at pH 3 + 5 M GdnSCN	2.22						1.33

^a The general experimental conditions are given in the legend to Figure 1. The uncertainties in the values of τ_1 and τ_2 are about 5%, and the uncertainty in the value of τ_3 is about 25%.

The distribution analysis of barstar at pH 7 and pH 3 are shown in Figure 1C. It can be seen that the distribution has two peaks at pH 7 and three peaks at pH 3, and the peak positions are consistent with the lifetimes obtained by the discrete analysis. It is important to realize that no functional form has been assumed in the lifetime distribution analysis by the maximum entropy method (see Experimental Section). This is unlike in the case of earlier studies^{33,34} where some specific functions were assumed in fitting the data. Due to computational restrictions, distribution analysis was carried out only in specific cases (see below). The good match observed between the lifetimes obtained in the discrete analysis and the average lifetimes of the corresponding peaks in the distribution analysis validates the use of discrete analysis in all the situations.

The appearance of the short (~ 0.2 -ns) component was pH dependent. Figure 2 shows the increase in the contribution of the short lifetime component ($\alpha_3\tau_3/\tau_m$) to the intensity with decreasing

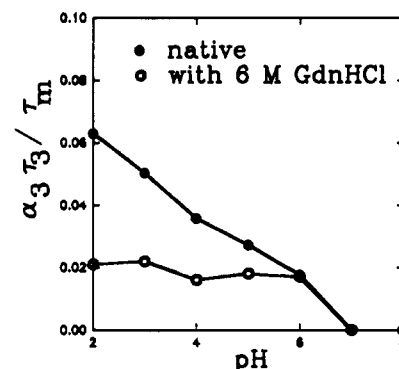


Figure 2. Dependence of the contribution ($\alpha_3\tau_3/\tau_m$) of the very short lifetime (~ 0.2 -ns) component with pH in the presence (O) and in the absence (●) of 6 M GdnHCl. The decay profiles were analyzed independently. At pH 7 and 8, the decay was biexponential. The buffer consisted of a mixture of 10 mM sodium dihydrogen phosphate, 10 mM trisodium citrate, and 10 mM sodium borate, adjusted to the desired pH. Other conditions were similar to those given in Figure 1.

pH. In this case, three exponential fits were performed at all the pH values below 7. The pK_a of the titration was around 4.5. Figure 3 shows the pH dependence of the value of the longest lifetime (τ_1). This also shows a transition around pH 4.5. The model compound *N*-acetyl-L-tryptophanamide (NATA), however, showed only a small (5%) decrease in lifetime from pH 7 to pH 3 (Figure 3).

Fluorescence Decay in the Presence of Denaturants. In the presence of the denaturant GdnHCl (6 M), the longest lifetime component (~ 4 ns) showed a marked decrease, indicating the collapse of tertiary structure (Table 1). In this case also, three exponentials were required to obtain a good fit at pH 3 with 6 M GdnHCl. Also shown are the effects of other denaturants such as 8 M urea and 5 M guanidine isothiocyanate (GdnSCN) (Table 1). The lifetimes observed in the presence of these denaturants are different from those observed with 6 M GdnHCl; this is because, unlike GdnHCl, they affect the fluorescence decay of Trp as observed by our studies with the model compound NATA

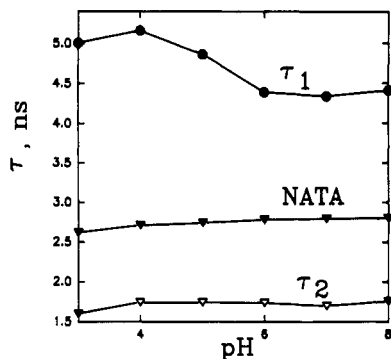


Figure 3. Dependence of fluorescence lifetimes τ_1 (~ 4 ns) and τ_2 (~ 1.5 ns) of barstar on pH. The behavior of the lifetime of the model compound NATA is also shown for comparison. The excitation and emission wavelengths for NATA were 295 and 360 nm, respectively. Other conditions were similar to those given in Figure 2. The decay was single exponential for NATA at all pH values.

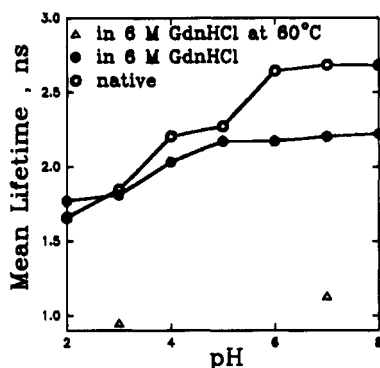


Figure 4. Dependence of the mean fluorescence lifetime, τ_m ($= \sum \alpha_i \tau_i$), of barstar on pH in the presence (●) and in the absence (○) of 6 M GdnHCl. The mean lifetime at 60 °C in the presence of 6 M GdnHCl (Δ) is shown for pH 3 and 7. The decay profiles were analyzed independently. Other conditions were similar to those given in Figure 2.

(Table 1). The lifetimes observed in the presence of 6 M GdnHCl were not significantly dependent on pH.

Figure 4 shows the change in the mean lifetime ($\tau_m = \sum \alpha_i \tau_i / \sum \alpha_i$) with pH in the presence and absence of 6 M GdnHCl. The increase in the mean lifetime with the increase in pH, in the native condition, implies the emergence of some definite three-dimensional structure. This increase was significantly (but not completely) reduced in the presence of 6 M GdnHCl (Figure 4). The increase in mean lifetime with pH was also observed at 60 °C in the presence of 6 M GdnHCl (Figure 4). The mean lifetime increased from 0.95 ns at pH 3 to 1.13 ns at pH 7.

Effect of the Mutation Cys → Ala in Barstar. Barstar has two cysteine residues (Cys-40 and Cys-82), and one of them (Cys-40) is two residues away from one of the Trp residues (Trp-38). The fluorescence decay characteristics of the Cys → Ala mutant (in which both cysteines were replaced by alanines) of barstar were compared with the wild-type barstar with the aim of obtaining some clues regarding the environment surrounding the Trp residues in barstar. Cysteine is known to quench Trp fluorescence.³⁵ The results are summarized in Table 2. It can be seen that mutant barstar has 42% more quantum yield (proportional to steady-state fluorescence intensity) compared to the wild type, both at pH 7 and pH 3. This difference in quantum yield was virtually absent when the protein was denatured with 6 M GdnHCl. This suggests that cysteine could be in the vicinity of at least one Trp in the tertiary/secondary structure of barstar. Between the wild type and the mutant, the changes in the mean lifetime (τ_m) were qualitatively similar to changes in the steady-state intensities (I), although the changes in the former were smaller (Table 2). This difference was more pronounced at pH

7 than at pH 3. This would indicate that the loss in the fluorescence intensity (I) at pH 7 arises mainly by static quenching with an immeasurably short lifetime. At pH 7, the wild type showed a decrease in the normalized amplitude of the 4-ns component when compared to the mutant. This could be due to partial quenching of the 4-ns decay component by SH group(s) in the wild type.

Fluorescence Quenching by KI and Acrylamide. The quenching of fluorescence of barstar by acrylamide and KI was studied under various experimental conditions by monitoring the time-resolved fluorescence at various quencher concentrations. Stern-Volmer plots for quenching by KI are shown in Figure 5. No significant quenching was observed at pH 7 for all the lifetimes. This indicates that the Trp residue(s) is not accessible to solvent at pH 7. The quenching rate constant, k_q , for the mean lifetime was $\sim 8 \times 10^7 \text{ M}^{-1} \text{ s}^{-1}$. At pH 3, the level of quenching was significantly higher than that observed at pH 7, indicating increased exposure of Trp residues to solvent. At pH 3, the mean lifetime displayed a sharp decrease at low concentration and a tendency to saturate above 400 mM KI (Figure 5B), suggesting that at least one of the Trp residues is more accessible to solvent than others. In the presence of 6 M GdnHCl, the quenching was more efficient at both pH 3 and pH 7 as expected (data not shown). Also, the quenching pattern (τ_0/τ vs [KI] plots) by KI at both pH values was similar in the presence of 6 M GdnHCl (data not shown).

Acrylamide was found to be a more efficient quencher compared to KI (Figure 6). The more efficient quenching by acrylamide could be due to its ability to access partially buried Trp residues. The pattern of acrylamide quenching at pH 7 indicates that the short lifetime component (1.5 ns) is quenched more effectively when compared to the long lifetime component (4 ns), and the normalized amplitudes did not vary significantly with the quencher concentration (data not shown). Also, the Stern-Volmer (S-V) plot for the short lifetime component was linear, whereas it was nonlinear in the case of the long lifetime component (Figure 6A). k_q was $\sim 1 \times 10^9 \text{ M}^{-1} \text{ s}^{-1}$ in the case of the short lifetime component. The nonlinear S-V plot seen in the case of the long lifetime was fitted to a model with two populations of Trp residues having similar lifetimes (see Appendix and Figure 6A) but differing in their accessibility to acrylamide. The k_q values for the two populations were calculated to be $\sim 4 \times 10^9$ and $\sim 1 \times 10^7 \text{ M}^{-1} \text{ s}^{-1}$. The relative contributions of the two populations to the emission intensity were 0.17 and 0.83, respectively. This analysis suggests that the long lifetime component (4 ns) arises mainly from a group of two Trp residues and the short lifetime (1.5 ns) is due to the third Trp residue. Also, one of the two Trp residues contributing to the long lifetime is accessible to acrylamide (with $k_q \sim 4 \times 10^9 \text{ M}^{-1} \text{ s}^{-1}$), and the other is deeply buried ($k_q \sim 1 \times 10^7 \text{ M}^{-1} \text{ s}^{-1}$). The k_q value of $1 \times 10^9 \text{ M}^{-1} \text{ s}^{-1}$ obtained for the short lifetime indicates this component to be accessible to acrylamide. Solvent-exposed Trp residues in several proteins have k_q (with acrylamide) values in the range $(3-4) \times 10^9 \text{ M}^{-1} \text{ s}^{-1}$.³⁶ Hence, the value of $1 \times 10^9 \text{ M}^{-1} \text{ s}^{-1}$ obtained for the 1.5-ns decay component would suggest a partially buried situation.

The preferential quenching of the short (1.5-ns) component at pH 7 can be seen very clearly in the distribution analysis (Figure 1C). The peak corresponding to the short component shifted to lower τ values with increasing concentration of acrylamide. The behavior of the other peak (4 ns) is quite interesting. A part of this peak was quenched and appeared as another component at moderate (~ 400 mM) levels of acrylamide (Figure 1C). The resolution of the 4-ns peak into two components agrees with the two-component analysis of the nonlinear Stern-Volmer plots for this decay component (Figure 6A). At higher concentrations of acrylamide (~ 800 mM), the middle component was absent probably as the result of merger into the quenched 1.5-ns component. Thus, the analysis by lifetime distribution supports the conclusion that the shorter lifetime (1.5-ns) component

TABLE 2: Comparison of Fluorescence Decay Characteristics of the Cys → Ala Mutant (Mut) of Barstar with That of the Wild Type (WT)^a

conditions	τ_m , ^b	I^c	lifetimes, ns			amplitudes			χ^2_{red}
			τ_1	τ_2	τ_3	α_1	α_2	α_3	
1. WT, pH 7	2.75	1.00	4.11	1.46		0.49	0.51		1.28
2. Mut, pH 7	3.16	1.42	4.11	1.55		0.63	0.37		1.16
3. WT, pH 7, 6 M GdnHCl	2.41	1.00	3.57	1.38		0.47	0.53		1.39
4. Mut, pH 7, 6 M GdnHCl	2.46	1.06	3.55	1.37		0.50	0.50		1.50
5. WT, pH 3	1.76	1.00	4.88	1.48	0.20	0.21	0.46	0.33	1.15
6. Mut, pH 3	2.31	1.42	5.14	1.70	0.24	0.28	0.46	0.26	1.03
7. WT, pH 3, 6 M GdnHCl	1.83	1.00	3.53	1.55	0.24	0.28	0.51	0.21	1.07
8. Mut, pH 3, 6 M GdnHCl	1.83	1.14	3.53	1.53	0.16	0.30	0.48	0.22	1.03

^a The experimental conditions are given in the legend to Figure 1. ^b Mean lifetime ($=\sum_i \alpha_i \tau_i$). ^c The steady-state intensity, calculated from the integrated area of steady-state emission spectrum, relative to WT, for equal absorbance at the excitation wavelength $\lambda = 280$ nm.

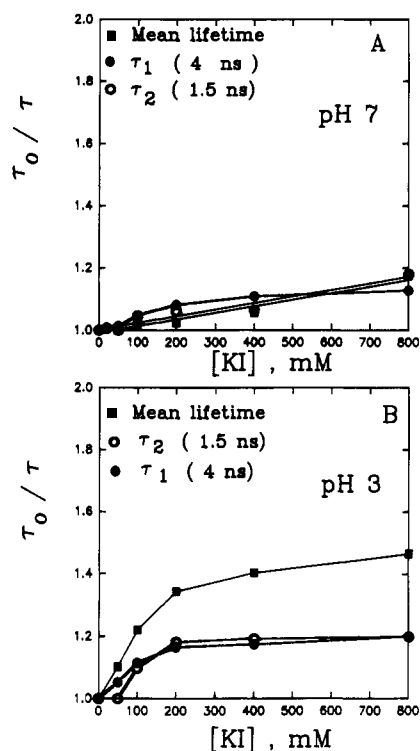


Figure 5. Stern-Volmer plots for the quenching of fluorescence lifetimes of barstar by KI at pH 7.0 (A) and pH 3.0 (B). τ_0 and τ are the lifetimes in the absence and in the presence of the quencher, respectively. τ_m (mean lifetime), ■; τ_1 (~4 ns), ●; and τ_2 (~1.5 ns) ○. The very short 0.2-ns component was not included due to large errors in its determination. The medium also contained $\text{Na}_2\text{S}_2\text{O}_3$ (100 μM) to avoid the formation of I_3^- . Other conditions are similar to those given in Figure 1.

represents the population of accessible fluorophores and the longer (4-ns) component is contributed by both buried and accessible populations of fluorophores.

Comparison of the pattern of quenching at pH 7 and 3 (Figure 6A and 6B) indicates the following: (i) The short lifetime (1.5-ns) component is quenched more effectively at pH 7 when compared to pH 3, indicating less accessibility of this component at pH 3; (ii) the mean lifetime (τ_m) decreased to a larger extent at pH 3, suggesting that the overall accessibility of the Trp residues is more at this pH. The latter observation is similar to that observed with KI (Figure 5).

Emission Wavelength Dependence of Fluorescence Decay. The fluorescence decay characteristics of barstar at pH 3 and 7 were observed as a function of the emission wavelength. The decay curves for a given pH at various emission wavelengths were analyzed globally to extract the wavelength-dependent amplitude parameters (see Experimental Section). The decay-associated spectra constructed from these are shown in Figure 7 (see Experimental Section). It can be seen that at pH 7, the long lifetime (4.0-ns) component showed a dominance and a maximum in the shorter wavelength region of the spectrum (Figure 7A).

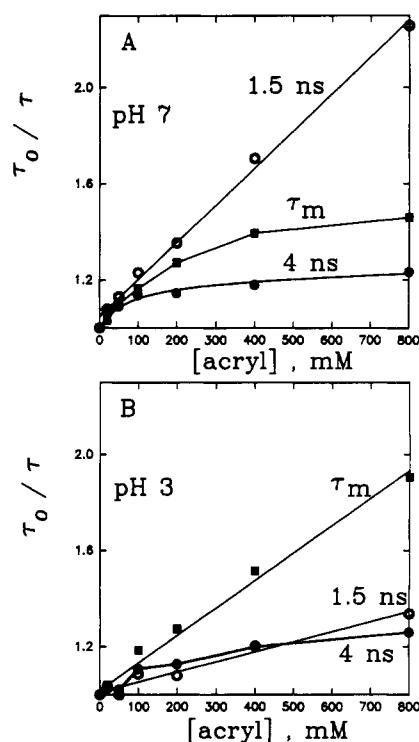


Figure 6. Stern-Volmer plots for the quenching of fluorescence lifetimes of barstar by acrylamide (acryl) at pH 7.0 (A) and pH 3.0 (B). The symbols stand for the same parameters as in Figure 5. The smooth line for the τ_1 at pH 7 (~4 ns) was simulated for a model having two populations with k_q values $\sim 4 \times 10^9$ and $\sim 1 \times 10^7$ $\text{M}^{-1} \text{s}^{-1}$ and relative populations of 0.17 and 0.83, respectively, according to eq 5 in the Appendix. Other conditions are similar to those given in Figure 1.

The spectrum of the shorter lifetime (1.5-ns) component had its maximum red-shifted compared to the long lifetime component. These data suggest that the Trp residue(s) contributing to the long lifetime is in a more hydrophobic environment (and hence buried) compared to those contributing to the shorter lifetime. Fluorescence quenching by acrylamide had also indicated a similar picture (Figure 6A).

The decay-associated spectra at pH 3 were quite different when compared to pH 7 (Figure 7B). The long (4.9-ns) lifetime component had its spectra red-shifted when compared to pH 7 (Figure 7B), suggesting increased exposure to solvent. The short (1.5-ns) and the very short (0.2-ns) lifetime components showed maxima in the short wavelength region. The observed decrease in the quenching efficiency by acrylamide of the short (1.5-ns) component at pH 3 when compared to pH 7 (Figure 6) also supports the decrease in the accessibility of this component at pH 3.

Time-Resolved Fluorescence Anisotropy Studies. In order to get information on the dynamic aspects of the various structural forms, time-resolved fluorescence anisotropy (r) measurements were carried out. Typical decay curves at pH 7 and 3 are shown

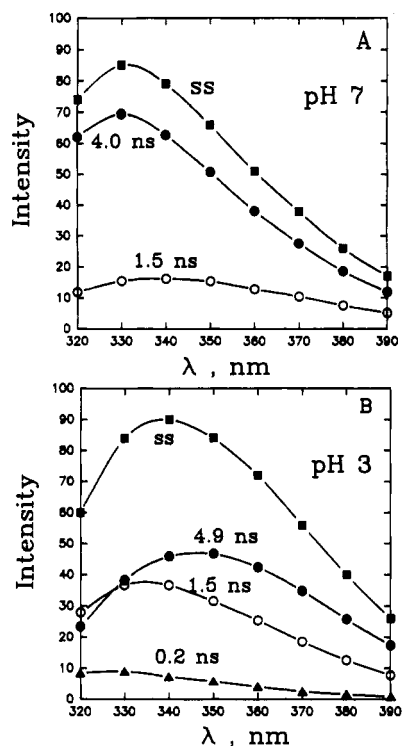


Figure 7. Decay-associated spectra (DAS) of individual decay components at pH 7.0 (A) and pH 3.0 (B). Emissions collected at various wavelengths were analyzed globally for the same fluorescence lifetimes but varying amplitude values in order to construct the DAS (see Experimental Section). The steady-state (ss) emission spectra are also shown for comparison. Other experimental conditions are similar to those given in Figure 1.

in Figure 8. To enhance the clarity and avoid crowding, the decay curves have been shifted (see legend) in the Y axis. It can be seen that, in the absence of any denaturant, the decay pattern at pH 3 is quite different from that at pH 7. Whereas the fluorescence anisotropy showed a tendency to decay back to zero at pH 7, it showed a tendency to level off to a non-zero value of r (called r_{∞}) at pH 3. A plot of β_2 obtained at various pH values showed a transition at \sim pH 4.5 (data not shown) similar to earlier titrations (Figure 2).

Analysis of the fluorescence anisotropy decay curves (see Experimental Section for the model) shows that the curve could be fitted to a single rotational correlation time (τ_r) of \sim 4.1 ns (Table 3) at pH 7. In contrast, at pH 3, the fitting required two correlation times of \sim 1.1 ns and another very long (>50 ns) which would lead to non-zero value of $r(r_{\infty})$ during our observation time window of 10–15 ns. The value of τ_r (4.1 ns) obtained at pH 7 is associated with the rotational dynamics of the whole protein. This interpretation agrees fairly well with the theoretically calculated³⁷ value of 3.6 ns for a hydrated globular protein of molecular weight 10 100 in aqueous medium at 25 °C. This could indicate that the surroundings of the Trp residues in barstar are quite structured and devoid of any segmental mobility at pH 7. The smaller value (\sim 1.1 ns) of τ_r at pH 3 would demand either segmental mobility or random coil state around Trp residue(s).

The second and much longer value (>50 ns) of τ_r seen at pH 3 is quite surprising. The value of $\tau_r > 50$ ns cannot be correlated with a monomeric protein even after the inclusion of three layers of hydration shells. The most likely explanation is the presence of the aggregated state of this protein at this pH. Assuming a globular shape for this aggregate, we could say that the average molecular weight of this aggregate would be >50 000. Subsequent sedimentation velocity measurements have indicated a monomer at pH 7 and an aggregate of \sim 160 000 at pH 3 (Khurana and Udgaonkar, unpublished observations). The aggregated state at pH 3 is seen in gel filtration experiments also (Khurana and

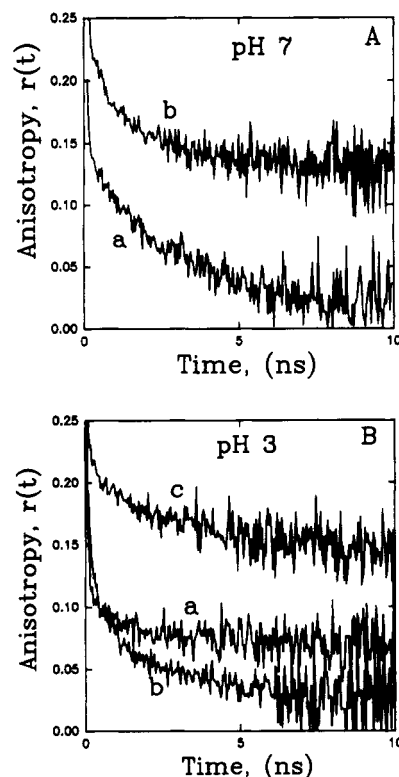


Figure 8. Decays of fluorescence anisotropy of barstar at pH 7.0 (A) and pH 3.0 (B). Other conditions are similar to those given in Figure 1. Decays in the absence (a) and in the presence (b) of 6 M GdnHCl are shown. Trace c (in B) shows the decay in the case of the Cys \rightarrow Ala mutant at pH 3.0 in the absence of GdnHCl. The traces are shifted along the Y axis in order to avoid congestion. The shifts are as follows: (A) 0.0 for trace a and +0.1 for trace b; (B) 0.0 for trace a, 0.0 for trace b, and +0.1 for trace c. Note that the anisotropy tends to saturate to non-zero values (r_{∞}) in the presence of 6 M GdnHCl (traces b).

TABLE 3: Parameters Associated with the Decay of Fluorescence Anisotropy of the Wild Type (WT) and the Cys \rightarrow Ala Mutant (Mut) Barstar^a

condition	τ_0	τ_{r1} , ns	τ_{r2} , ns	β_1	β_2	χ^2_{red}
1. WT, pH 7	0.12	4.1		1.0		1.75
2. WT, pH 3	0.10	1.1	>50	0.26	0.74	1.59
3. WT, pH 3, 0.2 M KCl	0.12	1.2	>50	0.26	0.74	1.75
4. Mut, pH 3	0.11	1.0	22	0.36	0.64	1.36
5. Mut, pH 3, 0.2 M KCl	0.11	1.0	33	0.34	0.66	1.70
6. WT, pH 7, 6 M GdnHCl	0.09	2.0	∞	0.92	0.08	1.52
7. WT, pH 3, 6 M GdnHCl	0.10	1.0	∞	0.79	0.21	1.28

^a See the legend to Figure 1 for general experimental conditions and Experimental Section for the model used in the analysis.

Udgaonkar, unpublished results). The relative proportion (β_1 and β_2) of the two rotational correlation times seen at pH 3 was independent of the ionic strength of the medium in the range 10–210 mM (Table 3). This rules out any electrostatic interaction as the driving force for the aggregation. In the case of the Cys \rightarrow Ala mutant, at pH 3, the longer component τ_{r2} was significantly shorter than that observed in the wild type and could be measured with a fair level of accuracy (Figure 8 and Table 3). The value of τ_{r2} (\sim 20 ns) observed in this case indicates again the presence of aggregates. However, the significantly smaller value of τ_{r2} when compared to the wild type indicates that either the average size of aggregates or the extent of aggregation is small. It is significant to note that, in this case also, neither τ_{r2} nor β_2 was dependent on ionic strength (Table 3).

In the presence of 6 M GdnHCl, the anisotropy decay could be fitted well to a correlation time of 1–2 ns ($\beta = 0.8$ –0.9) and r_{∞} component, in all cases. This shows that the aggregates formed at pH 3 could be broken up by denaturants. The value of τ_r (1–2 ns) obtained in these cases is similar to those obtained with other

denatured proteins.^{38,39} The titration of β_2 with increasing concentration of GdnHCl showed a transition (from 0.74 to 0.21) with midpoint around 3 M GdnHCl at pH 3 (data not shown). Thus, this transition agrees well with the steady-state unfolding studies at pH 3.¹³

Discussion

Barstar is an ideal protein for folding studies because of its small size (10 100), solubility in aqueous media, and the ease with which it can be cloned, expressed, and purified.⁴⁰ The crystal structure of the Cys \rightarrow Ala mutant of barstar complexed with barnase has been solved recently.⁴¹ Recent studies by one of us has shown that barstar could exist in two conformations, N (native) state and A (acid) form, the A form being stabilized at pH values below 4.¹³ It was also shown that the A form, which resembles the molten globule, has $\sim 60\%$ of the secondary structure of the N state. Since molten globule-like forms could be early intermediates in protein folding, structural and dynamic studies of this conformation have attracted several workers.^{7,10,42} We have used the intrinsic fluorescence of the three Trp residues of barstar to get structural and dynamic information on the molten globule-like A form as well as the native (N) state.

Time-resolved intrinsic fluorescence studies in proteins have been complicated by the multiexponential nature of fluorescence decay even in proteins with a single Trp residue.^{14,15,43-52} Hence, the assignment of the fluorescence lifetimes obtained in the case of barstar, which has three Trp residues, to any single Trp residue is not straightforward. Multiple exponential decay of Trp fluorescence has been generally attributed to multiple conformations (rotamers) of Trp residues,^{53,45} multiple microstates of proteins,⁵⁰ or multiple structures of the protein.^{43,52} Site-directed mutagenesis has been used in some cases to assign the lifetimes to individual Trp residues in multiple Trp proteins.^{46,54} Also, selective photolysis of the exposed Trp residue has been used to associate individual decay components to individual Trp residues in native α -crystallin.⁵⁵

Barstar, at pH 7, has fluorescence lifetimes of ~ 4.1 and ~ 1.5 ns, while at pH 3 the lifetimes are ~ 4.9 , ~ 1.5 , and ~ 0.2 ns. Quenching of fluorescence by KI (Figure 5) has shown that none of the Trp residues is solvent exposed at pH 7. Quenching by acrylamide (Figure 6) has suggested that the 1.5-ns decay component represents a fairly accessible population of Trp residues, while the ~ 4 -ns component is contributed by two populations, one accessible and the other buried. Hence, it is very likely that the ~ 1.5 -ns decay arises from one of the three Trp residues and the ~ 4 -ns decay corresponds to the other two. Thus, our analysis of fluorescence quenching has suggested a method of identifying the individual decay components with either an individual or a group of Trp populations. The buried nature of one of the populations contributing to the 4-ns decay is also supported by its decay associated spectra which showed a dominance in the blue region at pH 7 (Figure 7A). Although we have associated the three populations identified from quenching studies to the three Trp residues, we cannot rule out multiple conformations of either the Trp side chains or the entire protein. In this situation, each population may have contributions from more than one particular Trp residue.

The pH dependence of the decay parameters of barstar in the native state (Figures 2-4) reveals an apparent pK_a of ~ 4.5 , which is consistent with the steady-state measurements.¹³ In the presence of the denaturant GdnHCl, the pH dependence of the decay parameters was much less pronounced (Figures 2 and 4). The mean lifetime increases 1.22 times on going from pH 3 to pH 7. A similar increase (1.19 times) was also observed at 60 °C. Under denaturing conditions, one expects that the protein is in the random coil state, and the pH dependence is most likely to arise from the

pH titration of side chains of residues which are near/next to Trp. The likely residues in barstar are Asp-39 and Glu-52, which are next to Trp-38 and Trp-53, respectively. Residual structures under denaturing conditions have been reported recently in other proteins.^{56,57} The fluorescence experimental results do not rule out the presence of such residual structures for barstar in 6 M GdnHCl at 25 or 60 °C.

The increase in the mean lifetime (τ_m) in the Cys \rightarrow Ala mutant when compared to the wild type (Table 2) suggests that the cysteine residue(s) could quench the Trp fluorescence. This mutant has been shown to be active, although its complex with barnase is less stable than that of the wild type.⁵⁸ Both τ_m and the steady-state fluorescence intensity did not show significant change in the mutant in the presence of 6 M GdnHCl (Table 2). This indicates that the quenching by cysteine residue(s) arises due to their proximity to at least one Trp residue in the native structure.

The time-resolved fluorescence and anisotropy studies have brought out some distinct differences in the native (N) state and the low pH (A) form of barstar. The emergence of the very short lifetime (~ 0.2 -ns) component at lower pH and the $\sim 20\%$ increase in the long lifetime (~ 4 -ns) component at pH 3 also indicate that the structures at pH 3 and 7 are quite different from each other. These changes observed at pH 3 were not observed with some randomly selected other proteins such as hen eggwhite lysozyme, myelin basic protein, and melittin (data not shown). The origin of the ~ 0.2 -ns decay component observed at low pH (~ 3) could lie in a more dynamic state of the A form. The increased mobility could lead to population of states (e.g., rotamers of tryptophan), which would result in a short lifetime.

The decay-associated spectra of the long lifetime component underwent a red shift when the pH was changed from 7 to 3 (Figure 7). This suggests an increased exposure to solvent as expected for a dynamic molten globule-like state. The increased level of fluorescence quenching (as seen in the mean lifetime, τ_m) observed at pH 3 when compared to pH 7 (Figures 5 and 6), by both KI and acrylamide, also shows that the structure in general is more open in the A form. In fact, molten globule-like structures are characterized by a high level of openness with very little tertiary interactions.⁷ Thus, the fluorescence intensity decay studies at pH 7 and 3 do indeed bring out the special nature of the structure of the A form.

The fluorescence anisotropy decay has given further information on the A form of barstar in comparison to its native form. The rotational correlation time of 4.1 ns observed at pH 7 (Table 3) is consistent with the theoretically calculated value (3.6 ns) for a hydrated globular protein of molecular weight 10 100. This implies a rigid environment for all the Trp residues and the absence of any segmental mobility near the Trp residues. This, in turn, would imply a buried and solvent inaccessible nature for all the Trp residues. In fact, the absence of significant quenching by KI had also suggested a similar picture.

At pH 3, the fluorescence anisotropy decay gave at least two correlation times of 1.1 and >50 ns. The short correlation time (τ_{r1}) of 1.1 ns observed in the A form could be due to a high level of segmental mobility (which was absent at pH 7) around the Trp residue(s). The segmental mobility would allow a restricted rotation of the Trp residues. If one assumes that the rotational dynamics of the Trp residue is confined to a cone, then the semiangle of the cone can be calculated from the $r_\infty (= \beta_2 r_0)$ value.²⁵ The calculated value of the semiangle is 26° at pH 3. A value of 90° indicates free rotation of the Trp. The value of τ_{r1} obtained at pH 3 is quite close to that observed in the presence of 6 M GdnHCl. The very long correlation time ($\tau_{r2} > 50$ ns) observed at pH 3 deserves some special comments. Any correlation time of >10 ns cannot be explained by a monomer protein of molecular

weight 10 100 even after including three layers of hydration shells. Hence, the observed long correlation time (>50 ns) almost certainly would indicate the presence of very high molecular weight aggregates. The absence of concentration dependence (in the range 30–300 μM) of decay of fluorescence anisotropy at pH 3 (data not shown) shows that the driving force for aggregation in the A form is quite strong, resulting in aggregation even at the lowest concentration used. Also the aggregates are unlikely to be stabilized by an electrostatic interaction as shown by the absence of ionic strength dependence of the amplitude associated with the long (>50-ns) correlation time (Table 3). Hydrophobic interaction of the (partially) exposed interior surfaces could be the factor responsible for aggregation. Exposure of hydrophobic interior in the A form was suggested by the binding of 1-anilino-8-naphthalene sulfonate.¹³

It is interesting to note that the Cys \rightarrow Ala mutant had a significantly lower value of τ_{r2} (~ 20 ns), indicating a much reduced level of aggregation in the A form (Table 3). Since the experimental medium had a high concentration of dithiothreitol in all our samples, it is unlikely that the increased level of aggregation in the wild type is due to any intermolecular disulfide bridge. Also, the reversibility of the pH titration in the wild type rules out any disulfide bond formation. It is likely that the cysteine SH group(s) is involved in aggregation by forming intermolecular H bonds.

The reduced level of quenching of the 1.5-ns component, by acrylamide, at pH 3 when compared to pH 7 is also explained by the aggregate nature of the A form. The requirement of higher concentrations of GdnHCl to melt the structure in the A form when compared to the N state¹³ is also due to aggregation in the A form.

It is interesting to note that the anisotropy does not decay back to zero in the presence of GdnHCl at both pH 7 and pH 3. This is likely to be due to hindrance, offered by a long polypeptide chain, to the free rotation of the Trp side chains. In the presence of 6 M GdnHCl, the cone semiangle was 66° at pH 7 and 54° at pH 3, indicating a relatively free rotation in the denatured state. The increased restriction to rotation at pH 3 could be the result of some residual level of aggregation even in the presence of GdnHCl.

An interesting question arises as to whether GdnHCl disrupts the aggregation before unfolding of the protein at pH 3. The near identical transition (with midpoint ~ 3 M GdnHCl) observed during the unfolding process¹³ and in the amplitude associated with the long correlation time (β_2) argues against this possibility. Thus, it is likely that the process of structural unfolding leads to the dissociation of the aggregates.

The most significant finding of the present work is the identification of the nature of the A form. Although the fluorescence technique has been extensively used in characterizing the structural and dynamic aspects of many proteins in their native states, very little work has been carried out on their alternative structural forms. The importance of such work arises from the difficulty in characterizing these alternative forms either by X-ray crystallography or by NMR. Does the molten globule-like A form have an significance in the folding pathway of barstar? It could be argued that the highly aggregated A form may not be an intermediate in the folding pathway of barstar since any intermediate would have to be a monomer. Folding intermediates that aggregate have, however, been detected on the folding pathway of several proteins, and it is possible that aggregation of folding intermediates could be a manifestation of a facile interaction of the molten globule monomer with the hydrophobic surface of a chaperone⁵⁹ when the protein folds inside the living cell. The role of the A form on the folding pathway of barstar and its interaction with chaperones is currently under active investigation.

Appendix

Resolving Nonlinear Stern–Volmer Plots. The Stern–Volmer equation for dynamic quenching of fluorescence is given by

$$\frac{\tau_0}{\tau} = 1 + k_q \tau_0 [Q] \quad (\text{A1})$$

where τ_0 and τ are the lifetimes in the absence and in the presence of the quencher (Q), respectively. k_q is the bimolecular quenching rate constant.

When two populations of fluorophores have their lifetime values (τ_1 and τ_2) very close to each other but have different levels of accessibility by the quencher (characterized by k_{q1} and k_{q2} respectively), the observed lifetime is given by

$$\tau_{\text{obs}} = \alpha \tau_1 + (1 - \alpha) \tau_2 \quad (\text{A2})$$

where α is the fractional amplitude associated with τ_1 . Also we could write

$$\frac{\tau_0}{\alpha \tau_1} = \frac{1 + k_{q1} \tau_0 [Q]}{\alpha} \quad (\text{A3})$$

$$\frac{\tau_0}{(1 - \alpha) \tau_2} = \frac{1 + k_{q2} \tau_0 [Q]}{1 - \alpha} \quad (\text{A4})$$

for the two populations.

Equations A2, A3, and A4 give

$$\frac{\tau_{\text{obs}}}{\tau_0} = \frac{\alpha}{1 + k_{q1} \tau_0 [Q]} + \frac{1 - \alpha}{1 + k_{q2} \tau_0 [Q]} \quad (\text{A5})$$

This equation has been used to fit the nonlinear Stern–Volmer plot in Figure 6.

References and Notes

- Creighton, T. E. *Proc. Natl. Acad. Sci. U.S.A.* **1988**, *85*, 5082.
- Jaenicke, R. *Biochemistry* **1991**, *30*, 3147.
- Puitsyn, O. B. *FEBS Lett.* **1991**, *285*, 176.
- Kim, P. S.; Baldwin, R. L. *Annu. Rev. Biochem.* **1990**, *59*, 631.
- Udgaonkar, J. B.; Baldwin, R. L. *Nature* **1988**, *335*, 694.
- Roder, H.; Elöve, G. A.; Englander, S. W. *Nature* **1988**, *335*, 700.
- Haynie, D. T.; Freire, E. *Proteins: Struct. Funct., Genet.* **1993**, *16*, 115.
- Goto, Y.; Calciano, L. J.; Fink, A. L. *Proc. Natl. Acad. Sci. U.S.A.* **1990**, *87*, 573.
- Goto, Y.; Takahashi, N.; Fink, A. L. *Biochemistry* **1990**, *29*, 3480.
- Kuwajima, K. *Proteins: Struct., Funct., Genet.* **1989**, *6*, 87.
- Baldwin, R. L. *Chemtracts* **1991**, *2*, 379.
- Hartley, R. W.; Rogerson, D. L.; Smeaton, J. R. *Prep. Biochem.* **1972**, *2*, 243.
- Khurana, R.; Udgaonkar, J. B. *Biochemistry* **1994**, *33*, 106.
- Beechem, J. M.; Brand, L. *Annu. Rev. Biochem.* **1985**, *54*, 43.
- Tanaka, F.; Mataga, N. In *Dynamics and Mechanisms of Photo-induced Transfer and Related Phenomena*; Mataga, N., Okada, T., Masuhara, H., Eds.; Elsevier Science: Amsterdam, 1992; pp 501–512.
- Periasamy, N.; Doraiswamy, S.; Maiya, G. B.; Venkataraman, B. *J. Chem. Phys.* **1988**, *88*, 1638.
- Banker, K. V.; Bhagat, V. R.; Das, R.; Doraiswamy, S.; Ghangrekar, A. S.; Kamat, D. S.; Periasamy, N.; Srivatsavoy, V. J. P.; Venkataraman, B. *Indian J. Pure Appl. Phys.* **1989**, *27*, 416.
- Skilling, J.; Bryan, R. K. *Mon. Not. R. Astr. Soc.* **1984**, *211*, 111.
- Livesey, A. K.; Brochon, J. C. *Biophys. J.* **1987**, *52*, 693.
- Bevington, P. R. *Data reduction and error analysis for the physical sciences*; McGraw-Hill: New York, 1969.
- Knutson, J. R.; Beechem, J. M.; Brand, L. *Chem. Phys. Lett.* **1983**, *102*, 501.
- Das, T. K.; Periasamy, N.; Krishnamoorthy, G. *Biophys. J.* **1993**, *64*, 1122.
- Kinosita, K. J.; Kawato, S.; Ikegami, A. *Biophys. J.* **1977**, *20*, 289.
- Donzel, B.; Gauduchon, P.; Wahl, P. *J. Am. Chem. Soc.* **1974**, *96*, 801.
- Lakowicz, J. R. *Principles of Fluorescence Spectroscopy*; Plenum: New York, 1983.
- Alcala, J. R.; Gratton, E.; Prendergast, F. G. *Biophys. J.* **1987**, *51*, 925.
- James, D. R.; Ware, W. R. *Chem. Phys. Lett.* **1986**, *126*, 7.

- (28) James, D. R.; Turnbull, J. R.; Wagner, B. D.; Ware, W. R.; Petersen, N. O. *Biochemistry* **1987**, *26*, 6272.
- (29) Eftink, M. R.; Ghiron, C. A. *Biophys. J.* **1987**, *52*, 467.
- (30) Gentin, M.; Vincent, M.; Brochon, J. C.; Livesey, A. K.; Cittanova, N.; Gallay, J. *Biochemistry* **1990**, *29*, 10405.
- (31) Bastiaens, P. I. H.; Hoek, A. V.; Benen, J. A. E.; Brochon, J.-C.; Visser, A. J. W. G. *Biophys. J.* **1992**, *63*, 839.
- (32) Alcalá, J. R.; Gratton, E.; Prendergast, F. G. *Biophys. J.* **1987**, *51*, 597.
- (33) Rosato, N.; Gratton, E.; Mei, G.; Finazzi-Agro, A. *Biophys. J.* **1990**, *58*, 817.
- (34) Bismuto, E.; Sirangelo, I.; Irace, G. *Arch. Biochem. Biophys.* **1991**, *291*, 38.
- (35) Demchenko, A. P. Biochemical Applications. In *Topics in Fluorescence Spectroscopy*; Lakowicz, J. R., Ed.; Plenum: New York, 1992; Vol. 3, pp 65-111.
- (36) Eftink, M. R. In *Topics in Fluorescence Spectroscopy*; Lakowicz, J. R., Ed.; Plenum: New York, 1991; Vol. 2, pp 53-126.
- (37) Cantor, C. R.; Schimmel, P. R. *Biophysical Chemistry*; W. H. Freeman and Co.: New York, 1980; Part 2.
- (38) Fernando, T.; Royer, C. A. *Biochemistry* **1992**, *31*, 6683.
- (39) Smith, C. J.; Clarke, A. R.; Chia, W. N.; Irons, L. I.; Atkinson, T.; Holbrook, J. J. *Biochemistry* **1991**, *30*, 1028.
- (40) Hartley, R. W. *J. Mol. Biol.* **1988**, *202*, 913.
- (41) Guillet, V.; Laphorn, A.; Hartley, R.; Mauguen, Y. *Structure* **1993**, *1*, 165.
- (42) Bismuto, E.; Gratton, E.; Sirangelo, I.; Irace, G. *Eur. J. Biochem.* **1993**, *218*, 213.
- (43) Chabbert, M.; Hillen, W.; Hansen, D.; Takahashi, M.; Bousquet, J.-A. *Biochemistry* **1992**, *31*, 1951.
- (44) Royer, C. A. *Biophys. J.* **1992**, *63*, 741.
- (45) Chen, L. X.-Q.; Longworth, J. W.; Fleming, G. R. *Biophys. J.* **1987**, *51*, 865.
- (46) Axelsen, P. H.; Bajzer, Z.; Prendergast, F. G.; Cottam, P. F.; Ho, C. *Biophys. J.* **1991**, *60*, 650.
- (47) Eftink, M. R.; Gryczynski, I.; Wiczak, W.; Laczko, G.; Lakowicz, J. R. *Biochemistry* **1991**, *30*, 8945.
- (48) Kulinski, T.; Visser, A. J. W. G.; O'Kane, D. J.; Lee, J. *Biochemistry* **1987**, *26*, 540.
- (49) Atkins, W. M.; Stayton, P. S.; Villafranca, J. J. *Biochemistry* **1991**, *30*, 3406.
- (50) Harris, D. L.; Hudson, B. S. *Biochemistry* **1990**, *29*, 5276.
- (51) Liao, R.; Wang, C.-K.; Cheung, H. C. *Biophys. J.* **1992**, *63*, 986.
- (52) Kim, S.-J.; Chowdhury, F. N.; Younathan, W. S. E. S.; Rosso, P. S.; Barkley, M. D. *Biophys. J.* **1993**, *65*, 215.
- (53) Chen, R. F.; Knutson, J. R.; Ziffer, H.; Porter, D. *Biochemistry* **1991**, *30*, 5184.
- (54) Locke, B. C.; MacInnis, J. M.; Qian, S.-J.; Gordon, J. I.; Li, E.; Fleming, G. R.; Yang, N.-C. *Biochemistry* **1992**, *31*, 2376.
- (55) Borkman, R. F.; Douhal, A.; Yoshihara, K. *Biochemistry* **1993**, *32*, 4787.
- (56) Dill, K. A.; Shortle, D. *Annu. Rev. Biochem.* **1991**, *60*, 795.
- (57) Neri, D.; Billeter, M.; Wider, G.; Wuthrich, K. *Science* **1992**, *257*, 1559.
- (58) Hartley, R. W. *Biochemistry* **1993**, *32*, 5978.
- (59) Martin, J.; Langer, T.; Boteva, R.; Schramel, A.; Horvich, A. L.; Hart, F. U. *Nature* **1991**, *352*, 36.